

Calculation of Static and Dynamic Stability Derivatives of the F/A-18E in Abrupt Wing Stall Using RANS and DES

James R. Forsythe¹, Charles M. Fremaux², and Robert M. Hall³

¹ Cobalt Solutions, LLC, Springfield, OH forsythe@cobaltcfd.com

² NASA Langley Research Center, Hampton, VA charles.m.fremaux@nasa.gov

³ NASA Langley Research Center, Hampton, VA robert.m.hall@nasa.gov

1 Introduction

During envelope expansion flights of the preproduction F/A-18E in the Engineering and Manufacturing Development phase, the aircraft encountered uncommanded lateral activity, which was labeled “wing drop”. An extensive resolution process was undertaken to resolve this issue. A production solution was developed, which included revising the flight control laws and the incorporation of a porous wing fold fairing to eliminate the wing drop tendencies of the pre-production F/A-18E/F. The wing drop events were traced to an abrupt wing stall (AWS) on one side of the wing causing a sudden and severe roll-off in the direction of the stalled wing. Development of a reliable computational tool for prediction of abrupt wing stall would enable designers to screen configurations prior to building the first prototype, reducing costs and limiting risks.

The preproduction F/A-18E provides an excellent testing ground for simulation tools due to the large amount of experimental data obtained.[1, 2] Previous computational research[3] focused on predicting the zero sideslip characteristics of the aircraft, including the break in the lift curve slope characteristic of AWS. It was found that by applying Detached-Eddy Simulation (DES) to this problem to predict the unsteady shock motion seen experimentally, a better mean flow prediction could be obtained, when compared to industry standard Reynolds-averaged (RANS) models.[4] Detached-Eddy Simulation is a hybrid RANS and LES model that for natural applications (i.e. applied as intended) uses RANS in the attached boundary layer, and LES elsewhere.[5, 6]

The current work seeks to extend the past computational successes to predicting stability derivatives (both static and dynamic) in the AWS regime. Both the Menter’s SST RANS and Spalart-Allmaras based Detached-Eddy Simulation were applied. To assess the accuracy of the simulations, comparisons are made against experiments.

In order to obtain approval for releasing this paper to the public, quantitative information has been removed from most vertical scales as per guidelines from the Department of Defense.

2 Governing Equations and Flow Solver

The commercial unstructured flow solver *Cobalt* was used[7]. The numerical method is a cell-centered finite-volume approach applicable to arbitrary cell topologies. The spatial operator uses an exact Riemann Solver, least squares gradient calculations using QR factorization to provide second-order accuracy in space, and TVD flux limiters to limit extremes at cell faces. A point implicit method using analytic first-order inviscid and viscous Jacobians is used for advancement of the discretized system. For time-accurate computations, a Newton sub-iteration scheme is employed, and the method is second-order accurate in time. The compressible Navier-Stokes equations were solved with an arbitrary Lagrangian Eulerian method to handle rigid body motion.

2.1 Menter’s Shear Stress Transport RANS model

In order to provide a baseline for comparison, computations were performed with the Menter’s Shear Stress Transport (SST) model[8]. The method is a blend of $k - \epsilon$ and $k - \omega$ models, using a parameter F_1 to switch from $k - \omega$ to $k - \epsilon$ in the wake region.

2.2 Detached-Eddy Simulation

The original DES formulation is based on a modification to the Spalart-Allmaras RANS model[9] such that the model reduces to its RANS formulation near solid surfaces and to a subgrid model away from the wall[5]. The DES formulation replaces in the S-A model the distance to the nearest wall, d , by \tilde{d} , where $\tilde{d} \equiv \min(d, C_{DES}\Delta)$. In “natural” applications of DES, the wall-parallel grid spacings are at least on the order of the boundary layer thickness and the S-A RANS model is retained throughout the boundary layer, i.e., $\tilde{d} = d$. Consequently, prediction of boundary layer separation is determined in the ‘RANS mode’ of DES. Away from solid boundaries, the closure is a one-equation model for the sub-grid-scale (SGS) eddy viscosity. When the production and destruction terms of the model are balanced, the length scale $\tilde{d} = C_{DES}\Delta$ in the LES region yields a Smagorinsky eddy viscosity $\tilde{\nu} \propto S\Delta^2$. The additional model constant $C_{DES} = 0.65$ was set in homogeneous turbulence, and was used in the following calculations.

For the current runs, the grid contained tight clustering around the wing fold fairing that reduced Δ enough to make the RANS-LES interface occur in the boundary layer. To remedy this situation, the DES length scale was modified according to the equation: $\tilde{d} = \min(C_{des} \max(n^2 C_{des} \Delta^2 / d, \Delta), d)$, where n is the ratio of the new RANS-LES interface height to the original height. Above the interface, the length scale draws down smoothly to $C_{des}\Delta$. For the current simulations $n = 3$ was chosen to push the interface outside of the boundary layer. Methods that detect the edge of the boundary layer would be far preferable to reduce the burden on the users.

3 Results

The configuration examined was an 8% scale pre-production F/A-18E with $6^\circ/8^\circ/4^\circ$ flaps set and flow through engines. The Mach number for all cases was 0.9, with a freestream static pressure and temperature of 8.575 psi and 518.5°R respectively, leading to a chord based Reynolds number of 3.90×10^6 . The wind tunnel comparisons are from the model tested in NASA Langley's 16 Ft Transonic Tunnel (16TT).

The grid used was unstructured, created using the tetrahedral grid generator VGRIDns[10]. The *Cobalt* utility *blacksmith* was used to recombine the high aspect ratio tetrahedra in the boundary layer into prisms. The grid was 8.4×10^6 cells for both sides of the aircraft. The average first y^+ for the grid was < 0.7 . The grid was created by performing a solution based adaptation using the time averaged results of a run at 9° angle of attack, using NASA Langley grid adaption code *RefineMesh* and the process described in reference [4]. Although the absolute number of cells would normally be considered quite coarse for a DES of a full aircraft, the grid cells were tightly clustered in the separation bubble because of the method of grid adaption.

3.1 Static Lateral Stability

Calculations were performed with various bank (ϕ) and pitch (θ) angles. RANS runs were performed using large timesteps to converge to steady state, while DES runs were run at a non-dimensional timestep (by chord and freestream velocity) of 0.01 (determined in reference [4]). Time-averages for the DES were taken over 120 non-dimensional time-units, which increased the cost of DES over RANS by about a factor of eight. For the experiments and computations, the pitch angle was held fixed, and the model rolled around the longitudinal axis of the aircraft. This leads to a reduction in alpha, and an increase in beta. Thus the calculations do not strictly give derivatives with respect to beta.

Figure 1 shows rolling moment vs. bank angle for four different pitch angles around the AWS regime. Note that for the experiments all four cases exhibit lateral static stability about $\phi = 0^\circ$. However, for the pitch angles greater than 7° , there are asymmetries in the data, and there appear to be significant rolling moments at zero bank. For the 9° case, model dynamics due to unsteady shock motion were strong enough to prevent taking a full set of data. The asymmetries and gaps in the experimental data make comparison difficult. All DES results predicted strong shock oscillations due to separation as was seen previously in [4] to give more realistic smeared mean pressure distributions. At $\theta = 7^\circ$ (Figure 1a) the SST RANS results (which show separation near the trailing edge at zero bank) are in good agreement for the low bank angles, but reverse sign at $\phi = 30^\circ$. Examination of flow visualizations showed this reversal to be caused by separation from the leading edge of the upwind wing. DES results for this angle showed a reduced

slope, likely caused by the fact that at this angle DES was separated further forward on the wing, in the mean. For the 8.5° and 10° cases there was a significant rolling moment at near zero bank for both the experiments and the DES. Running time averages of the DES rolling moment for 10° were examined and tended to stabilize at this non-zero moment despite averaging over one second of full scale time. So even if longer time-averages would tend towards zero, there is a rolling moment over a time significantly long enough to affect the aircraft motion. The RANS runs did not show this zero bank rolling moment, probably because the moment seems to be caused by low frequency shock oscillation, which was not captured in the RANS. Although not shown, yawing moment and side force were also plotted and compared to the experiments, with excellent agreement for both the RANS and DES. This is likely due to the fact that these coefficients are dominated by the flow around the vertical stabilizers, which is attached and easily predicted.

3.2 Dynamic Lateral Stability

Dynamic lateral stability was also examined by performing forced sinusoidal roll oscillations around the body axis. A roll rate was picked in order to stay low enough to be in the linear range as much as possible, yet have a large enough effect on the moments to be distinguishable from the effects of unsteady shock oscillation. An amplitude ($\pm 5^\circ$) and frequency were chosen to give a peak non-dimensional roll rate (when passing through wings level) that would induce an effective angle of attack change of 1° at the wingtip – i.e. $(\partial\phi/\partial t)b/2U_\infty = \tan(1^\circ) = 0.0175$. For both the RANS and DES a non-dimensional timestep of 0.02 was used, which was verified by a timestep study to be small enough to adequately resolve the motion. Since DES predicted strong shock oscillations, it was necessary to phase average over multiple cycles to obtain roll damping information. Most RANS cases gave the same (or nearly the same) results for two subsequent oscillations, so phase averaging was not required. So although the cost of the RANS and DES was the same per cycle (since both were run time-accurate), the cost of DES was higher due to the need to phase-average over multiple cycles.

Figure 2 plots the rolling moment vs. roll rate. The left and right hand sides of the loops correspond to when the aircraft is passing through wings level rolling either left or right respectively. Rolling moments of opposite sign to the roll rate yield stable roll damping (i.e. negative slope of a linear fit through the loops). The SST results exhibited stable roll damping in all cases, but for the 7° case had a significant rolling moment offset (i.e. a rolling moment with zero roll rate). This was seen from flow visualizations to be caused by the flow separating on one wing at the leading edge, and the other at the trailing edge. This is likely caused by the starting procedure which was to begin the simulation by rolling from wings level towards one side. A hysteresis effect could then allow that wing to stay separated while the other remained attached. The reduction in roll damping for angles above 7°

is caused by the drop in the lift curve slope once the flow separates from the leading edge of the wing. DES results showed highly non-linear rolling moments over each cycle and near zero roll damping (in a linear derivative sense) for 9° , although it would be useful to run more cycles to ensure that there are sufficient samples in the phase averages. At this angle (and the angles close to it) the variations in rolling moment due to shock unsteadiness are far stronger than the effect of the motion.

4 Conclusions

RANS and DES calculations were performed for the F/A-18E to predict static and dynamic stability derivatives in the challenging abrupt wing stall regime. Comparison to experiments for static stability derivatives demonstrated that DES picked up zero bank rolling moment offsets which could be a trigger for wing drop. DES also predicted a strong reduction of roll damping in the AWS regime that could also contribute to wing drop. More detailed comparisons to experiments is ongoing.

References

1. Lamar, J., Hall, R., "AWS Figures of Merit Developed Parameters from Static Transonic Model Tests," *AIAA 03-0745*, Jan 2003.
2. Owens, B., Brandon, J., Capone, F., Hall, R., Cunningham, K., "Free-to-Roll Analysis of Abrupt Wing Stall on Military Aircraft at Transonic Speeds," *AIAA 03-0750*, Jan 2003.
3. Woodson, S.H., Green, B.E., Chung, J.J., Grove, D.V., Parikh, P.C., Forsythe, J.R., "Recommendations for CFD Procedures for Predicting Abrupt Wing Stall," *AIAA 2003-0923*, Jan 2003.
4. Forsythe, J.R., Woodson, S.H., "Unsteady CFD Calculations of Abrupt Wing Stall using Detached-Eddy Simulation," *AIAA 2003-0594*, Jan 2003.
5. Spalart, P. R. , Jou W-H. , Strelets M. , and Allmaras, S. R., "Comments on the Feasibility of LES for Wings, and on a Hybrid RANS/LES Approach," *Advances in DNS/LES, 1st AFOSR Int. Conf. on DNS/LES*, Aug 4-8, 1997, Greyden Press, Columbus Oh.
6. Strelets, M., "Detached-Eddy Simulation of Massively Separated Flows," *AIAA 01-0879*, Jan 2001.
7. www.cobaltcfd.com
8. Menter, F.R., 1994, "Two-Equation Eddy-Viscosity Turbulence Models for Engineering Applications," *AIAA Journal*, 32(8), pp 1598–1605.
9. Spalart, P.R. and Allmaras, S.R., 1994, "A One-Equation Turbulence Model for Aerodynamic Flows," *La Recherche Aerospatiale* 1, pp. 5-21.
10. Pirzadeh, S., "Three-dimensional Unstructured Viscous Grids by the Advancing Layers Method," *AIAA Journal*, V. 34, pp. 43-49.

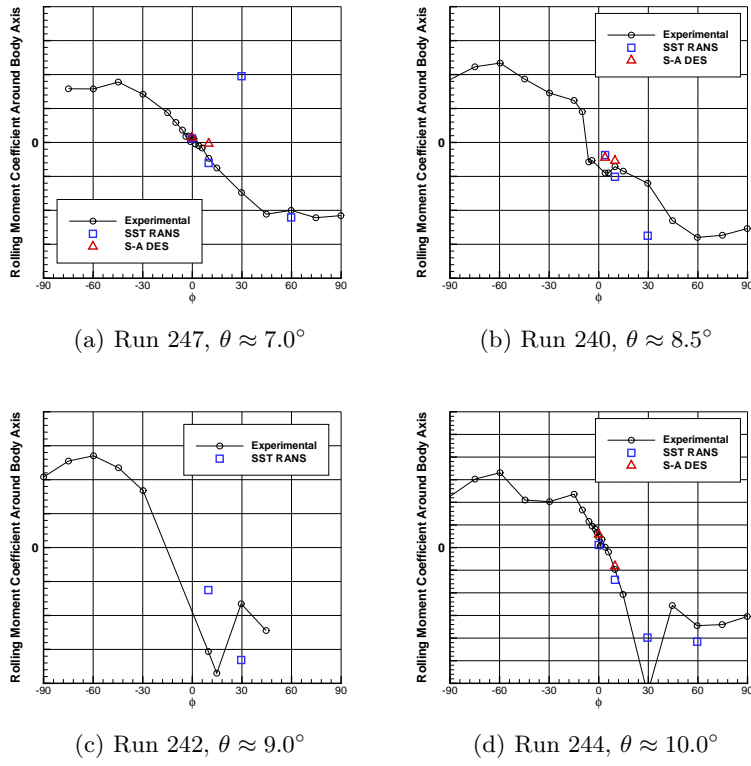


Fig. 1. Rolling moment coefficient vs. bank angle

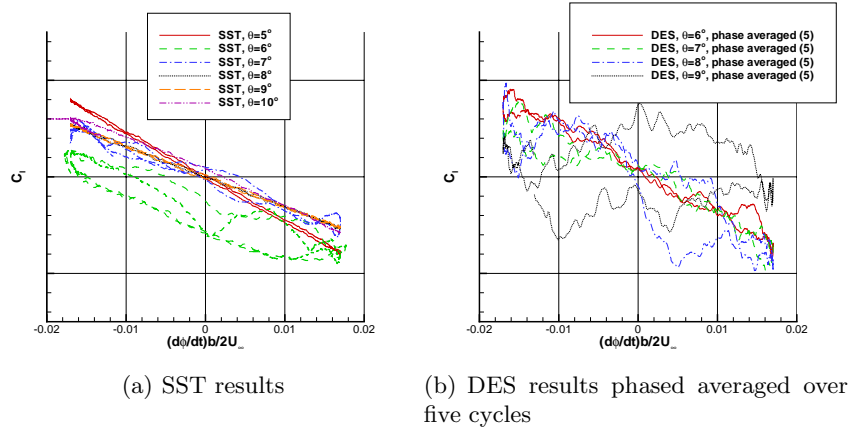


Fig. 2. Forced oscillation runs, rolling moment coefficient vs. roll rate